JACS
JOURNAL OF THE AMERICAN CHEMICAL SOCIETY
Article
pubs.acs.org/JACS

n-Type Semiconducting Naphthalene Diimide-Perylene Diimide Copolymers: Controlling Crystallinity, Blend Morphology, and Compatibility Toward High-Performance All-Polymer Solar Cells

Ye-Jin Hwang, Taeshik Earmme, Brett A. E. Courtright, Frank N. Eberle, and Samson A. Jenekhe*

Department of Chemical Engineering and Department of Chemistry, University of Washington, Seattle, Washington 98195-1750, United States

Supporting Information

ABSTRACT: Knowledge of the critical factors that determine compatibility, blend morphology, and performance of bulk heterojunction (BHJ) solar cells composed of an electron-accepting polymer and an electron-donating polymer remains limited. To test the idea that bulk crystallinity is such a critical factor, we have designed a series of new semiconducting naphthalene diimide (NDI)-selenophene/perylene diimide (PDI)-selenophene random copolymers, *x*PDI (10PDI, 30PDI, 50PDI), whose crystallinity varies with composition, and investigated them as electron acceptors in BHJ solar cells. Pairing of the reference crystalline (crystalline domain size L_c = 10.22 nm) NDI-selenophene copolymer (PNDIS-HD) with crystalline (L_c = 9.15 nm) benzodithiophene-thieno[3,4-*b*]thiophene copolymer (PBDTTT-CT) donor yields incompatible blends, whose BHJ solar cells have a power conversion efficiency (PCE) of 1.4%. However, pairing of the new 30PDI with optimal crystallinity (L_c = 5.11 nm) as acceptor with the same PBDTTT-CT donor yields compatible blends and all-polymer solar cells with enhanced performance (PCE = 6.3%, J_{sc} = 18.6 mA/cm^2, external quantum efficiency = 91%). These photovoltaic parameters observed in 30PDI:PBDTTT-CT devices are the best so far for all-polymer solar cells, while the short-circuit current (J_{sc}) and external quantum efficiency are even higher than reported values for [70]-fullerene:PBDTTT-CT solar cells. The morphology and bulk carrier mobilities of the polymer/polymer blends varied substantially with crystallinity of the acceptor polymer component and thus with the NDI/PDI copolymer composition. These results demonstrate that the crystallinity of a polymer component and thus compatibility, blend morphology, and efficiency of polymer/polymer blend solar cells can be controlled by molecular design.

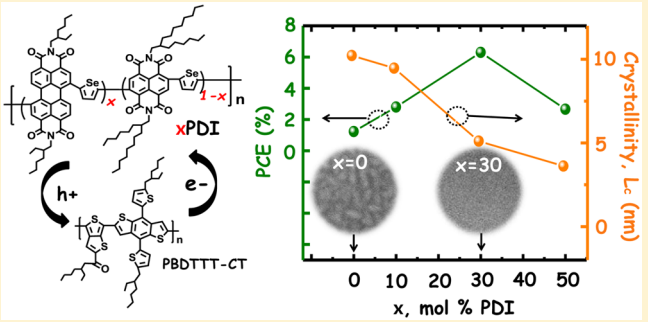

INTRODUCTION

All-polymer solar cells,[1] composed of an electron-donating polymer and an electron-accepting polymer components, are of growing interest because of their potential advantages over the more widely studied donor polymer/fullerene acceptor systems.[1,2] Although significant progress has been made in investigating and developing all-polymer solar cells, their performance in terms of the power conversion efficiency (PCE) of single-junction devices remains limited to about 5%,[3−6] while that of polymer/fullerene systems is over 9%.[7] One of the major challenges to further progress in developing highly efficient all-polymer solar cells is that besides having a suitable offset in the frontier molecular orbital (highest occupied molecular orbital/lowest unoccupied molecular orbital, HOMO/LUMO) energy levels of the polymer/polymer donor/acceptor pair, the other key factors that govern *compatibility* and blend morphology of the blend pair toward achieving efficient bulk heterojunction (BHJ) solar cells are not known or clear.[3−6,8] The longstanding useage of the term *compatibility* of a blend or *compatible blend* adapted here does not imply a specific scale of miscibility or microstructure in the blend but rather denotes a blend with enhanced or useful new properties compared to the components.[9] Furthermore, unlike universally applicable fullerene derivatives such as phenyl-C_{71}-butyric acid methyl ester ($PC_{71}BM$) and phenyl-C_{61}-butyric acid methyl ester ($PC_{61}BM$), current electron acceptor polymers are rarely compatible with multiple donor polymers in BHJ solar cells.[3−6] An important exemption to the universal compatibility of fullerene acceptors with multiple donor polymers (i.e., gives rise to high photovoltaic efficiency) is the indene-C_{60}-bisadduct, 1′,1″,4′,4″-tetrahydro-di[1,4]-methanonaphthaleno[1,2:2′,3′,56,60:2″,3″][5,6]fullerene-C_{60} (ICBA). ICBA is an amorphous material which is found to be only compatible with a very few semicrystalline polymers, notably poly(3-hexylthiophene) (P3HT)[10] and poly[(4,4′-bis(2-ethylhexyl)dithieno[3,2-*b*:2′,3′-*d*]silole)-2,6-diyl-*alt*-(2,5-bis(3-(2-ethylhexyl)thiophen-2-yl)thiazolo[5,4-*d*]thiazole)] (PSEHTT).[11] Studies of amorphous ICBA and crystalline fullerene acceptors ($PC_{61}BM$ and $PC_{71}BM$) with various donor

Received: December 30, 2014
Published: March 25, 2015

DOI: 10.1021/ja513260w
J. Am. Chem. Soc. 2015, 137, 4424−4434

polymers have led to the hypothesis that material crystallinity controls polymer/fullerene compatibility and blend microstructure and thus charge photogeneration efficiency and transport in such BHJ devices.[12] There are as yet no analogous or other studies of the role of crystallinity of the acceptor (or donor) polymer component on the compatibility, blend morphology, and performance of polymer/polymer BHJ solar cells.

In this paper we show that an incompatible polymer/polymer blend system with poor photovoltaic efficiency can be rendered compatible with over 4-fold enhancement in PCE by controlling the bulk crystallinity of the acceptor polymer while holding the donor polymer constant. Our initial studies of the reference all-polymer blend system, composed of a known crystalline electron-accepting NDI-selenophene copolymer PNDIS-HD[6] and a known crystalline benzodithiophene-thieno[3,4-*b*]thiophene copolymer (PBDTTT-CT)[13] donor (Chart 1) showed that the extensively optimized PNDIS-HD:PBDTTT-CT blend solar cells had PCEs of only 1.2−1.4%, and thus it constitutes an incompatible blend despite the very favorable HOMO/LUMO energy offset of the pair (Chart 1). To test the hypothesis that polymer crystallinity is a critical factor that controls the compatibility, blend morphology, and performance of polymer/polymer blend solar cells, we designed a series of new n-type semiconducting NDI-selenophene/PDI-selenophene random copolymers (Chart 1), *x*PDI (10PDI, 30PDI, 50PDI), in which the bulk crystallinity (e.g., mean crystalline domain size L_c determined by X-ray diffraction (XRD) analysis) decreased with increasing amount of PDI moiety substituted for NDI moiety in the reference PNDIS-HD. Pairing of the new 30PDI copolymer acceptor, which has a substantially decreased and optimal crystallinity, with PBDTTT-CT donor is found to give compatible blends and all-polymer solar cells with enhanced performance (PCE = 6.3%, J_{sc} = 18.6 mA/cm^2, external quantum efficiency (EQE) = 91%). Charge transport in neat films of the reference PNDIS-HD and the new NDI/PDI copolymers (10PDI, 30PDI, 50PDI) was investigated by using organic field-effect transistors (OFETs), and bulk charge transport in the polymer/polymer BHJ active layers was studied by the space-charge-limited current (SCLC) method. The surface and bulk morphologies of the PNDIS-HD/PBDTTT-CT and *x*PDI/PBDTTT-CT blend systems were investigated by atomic force microscopy (AFM) and transmission electron microscopy (TEM) imaging, respectively.

Chart 1. Molecular (a) and Electronic (b) Structure of PNDIS-HD, *x*PDI, and PDBTTT-CT

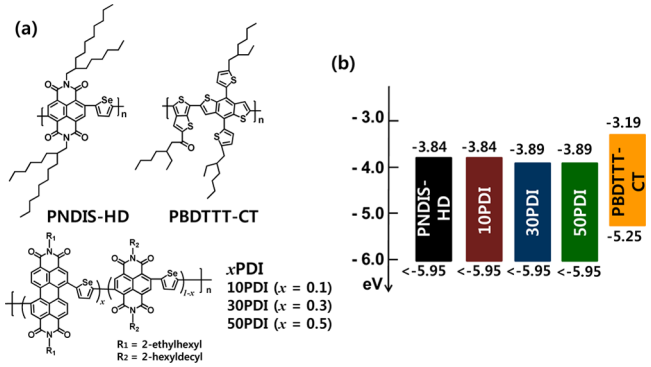

RESULTS AND DISCUSSIONS

Synthesis, Absorption Spectra, and Electronic Structure. The new n-type semiconducting, random, NDI-selenophene/PDI-selenophene copolymers denoted as *x*PDI, where *x* is the molar percentage of PDI-selenophene segments, were synthesized by Stille coupling copolymerization of three monomers, 4,9-dibromo-2,7-bis(2-hexyldecyl)benzo[*lmn*][3,8]-phenanthroline-1,3,6,8-tetraone (4,9-dibromo-NDI), *N*,*N*′-bis-(2-ethylhexyl)-1,7-dibromo-3,4,9,10-perylene diimide (1,7-dibromo-PDI), and 2,5-bis(trimethylstannyl)-selenophene (Scheme 1). The 4,9-dibromo-NDI and selenophene monomers were synthesized and purified by following our previous reports,[6] whereas the 1,7-dibromo-PDI monomer was obtained commercially (SunaTech Inc.) and was used without further purification. Three different compositions of *x*PDI, i.e. 10PDI, 30PDI, and 50PDI, were synthesized and investigated. In addition, the benchmark NDI-selenophene copolymer, PNDIS-HD,[6] as well as PDI-selenophene copolymer was also synthesized for the purpose of comparison. PNDIS-HD, 10PDI, 30PDI, and 50PDI showed good solubility (>30 mg/mL) in common organic solvents, including chloroform, chlorobenzene, and dichlorobenzene, at room temperature. However, PPDIS precipitated out during the polymerization and showed very limited solubility due to the short alkyl side chains, 2-ethylhexyl, and thus PPDIS was not further studied. The molecular structures of the monomers and copolymers were confirmed by ^{1}H NMR spectra (Figures S1−6). The molecular weight and polydispersity index (M_w/M_n) of the polymers were measured by gel permeation chromatography (GPC) against polystyrene standards in *o*-dichlorobenzene at 130 °C. The reference polymer, PNDIS-HD, had a weight-average molecular weight (M_w) of 42.6 kDa with M_w/M_n of 1.5. The M_w of *x*PDI was comparable with PNDIS-HD sample and was in the range of 32.1−57.2 kDa with a M_w/M_n of 1.3−1.4 (Table 1). Initially, GPC was performed in chlorobenzene at a lower temperature (60 °C), and *x*PDI showed significantly higher M_w in the range of 269.1−430.8 kDa with high M_w/M_n in the range of 2.6−3.5, indicating aggregation of the samples (Table S1). The p-type polymer PBDTTT-CT had M_n > 20 kDa with M_w/M_n ∼ 3. Thermogravimetric analysis (TGA) of all the n-type polymers showed good thermal stability with onset decomposition temperature (T_d) of over 400 °C under nitrogen flow (Figure S7).

Scheme 1. Synthesis of n-Type Semiconducting NDI/PDI Random Copolymers, *x*PDI

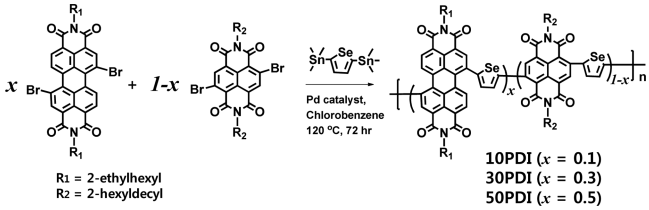

The optical absorption of the new NDI/PDI copolymers, *x*PDI, was characterized by UV−vis absorption spectroscopy of dilute (10^{-6} M) chloroform solutions (Figure 1a) and of thin films (95−110 nm) on glass substrates (Figure 1b). The optical absorption spectra of the reference PNDIS-HD acceptor and donor polymer, PBDTTT-CT, were also obtained for the purpose of comparison. In solution, *x*PDI materials showed two distinct absorption bands at 300−400 nm and 500−700 nm

DOI: 10.1021/ja513260w
J. Am. Chem. Soc. 2015, 137, 4424−4434

Table 1. Molecular Weight, Thin-Film Optical Absorption, Electronic Structure, and Field-Effect Electron Mobility of PNDIS-HD and *x*PDIs

polymer	M_w (kDa)	M_w/M_n	λ_{max} (nm)	E_g^{opt} (eV)	LUMO (eV)	μ_e ($cm^2/(V\ s)$)	V_{th} (V)	I_{on}/I_{off}
PNDIS-HD	42.6	1.5	348, 622	1.65	3.84	9.2×10^{-2}	10	10^3
10PDI	57.2	1.3	352, 615	1.70	3.84	5.5×10^{-2}	10	10^3
30PDI	52.5	1.4	349, 578	1.77	3.89	7.1×10^{-3}	5	10^3
50PDI	32.1	1.4	347, 544	1.77	3.89	4.0×10^{-3}	5	10^3

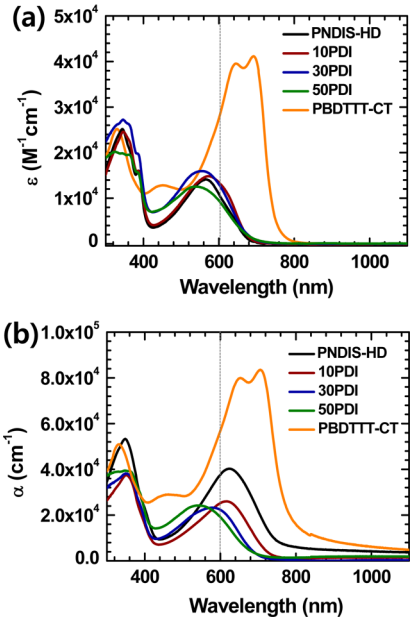

Figure 1. UV–vis absorption spectra of *x*PDI, PNDIS-HD, and PBDTTT-CT in dilute chloroform solution (a) and as thin films on glass substrates (b).

which can be assigned to $\pi-\pi^*$ or $n-\pi^*$ transition of the NDI and PDI chromophores and an intramolecular charge transfer (ICT) band, respectively. These absorption features are typically observed in NDI-based conjugated copolymers.[6,14] 10PDI has absorption maxima (λ_{max}) at 570 nm (maximum molar extinction coefficient, $\varepsilon_{max} = 1.48 \times 10^4\ M^{-1}\ cm^{-1}$) and at 346 nm ($\varepsilon_{max} = 2.46 \times 10^4\ M^{-1}\ cm^{-1}$) which are very similar to those of PNDIS-HD (λ_{max} = 568 and 344 nm). By increasing the amount of PDI moiety in the polymer backbone, however, the λ_{max} of the ICT band is blue-shifted to 555 nm ($\varepsilon_{max} = 1.59 \times 10^4\ M^{-1}\ cm^{-1}$) in 30PDI and to 539 nm ($\varepsilon_{max} = 1.25 \times 10^4\ M^{-1}\ cm^{-1}$) in 50PDI. The enhanced absorption near 500 nm in 30PDI and 50PDI originates from the PDI-selenophene moiety and can be explained by the fact that PDI copolymers typically have absorption maximum in the 500–560 nm range.[4] Our measured solution absorption spectrum of PBDTTT-CT has two peaks at 645 and 693 nm ($\varepsilon_{max} = 4.1 \times 10^4\ M^{-1}\ cm^{-1}$) with much higher molar extinction coefficient compared to the acceptor polymers. However, we note that the molar extinction coefficient of the new acceptor polymers, *x*PDI, is more than an order of magnitude higher than fullerene acceptors in the visible region.[15]

The thin-film absorption spectra are very similar to the solution spectra, but the longer wavelength (ICT) bands are red-shifted due to the increased conjugation and intermolecular interactions in the solid state. The reference PNDIS-HD has a visible region λ_{max} at 622 nm ($\alpha_{max} = 4.0 \times 10^4\ cm^{-1}$) which is 54 nm red-shifted compared to that in solution. An important consequence of the incorporation of PDI moieties into the n-type semiconducting copolymers, *x*PDI, is that the absorption coefficient is slightly lowered while the visible region absorption maximum λ_{max} progressively decreases from 615 nm ($\alpha_{max} = 2.6 \times 10^4\ cm^{-1}$) in 10PDI to 578 nm ($\alpha_{max} = 2.3 \times 10^4\ cm^{-1}$) in 30PDI and finally to 544 nm ($\alpha_{max} = 2.4 \times 10^4\ cm^{-1}$) in 50PDI. This trend is largely explained by the progressive decrease in planarity of the polymer backbone due to the increasing steric hindrance from the large PDI moiety. We note that the absorption maximum of 50PDI is already comparable to those of known PDI-containing alternating conjugated copolymers.[4] The measured α values for PNDIS-HD and *x*PDI are comparable with other reported NDI and PDI-based acceptor polymers.[3,4] The optical band gap (E_g^{opt}), determined from the onset absorption band edge of the acceptor polymers, increased from 1.65 eV in the reference PNDIS-HD to 1.70 eV in 10PDI and to 1.77 eV in 30PDI and 50PDI. Our measured thin-film absorption spectrum of PBDTTT-CT has an absorption maximum at 706 nm and E_g^{opt} of 1.55 eV, which are in good agreement with previous report of λ_{max} of 692 nm and E_g^{opt} of 1.58 eV.[13] Although the absorption coefficient of PBDTTT-CT is not previously reported, our measured α_{max} of $8.3 \times 10^4\ cm^{-1}$ in PBDTTT-CT is in good agreement with α_{max} values ($7 \times 10^4 - 9 \times 10^4\ cm^{-1}$) of other benzodithiophene-thieno[3,4-*b*]thiophene copolymers (PTB7 and PTB7-Th).[3b,f]

The electronic structures of the acceptor (*x*PDI, PNDIS-HD) and donor (PBDTTT-CT) polymers were investigated by using cyclic voltammetry (CV) of thin films. The ferrocene/ferrocenium (Fc/Fc^+) reference was used as an internal standard, which was assigned an absolute energy of −4.8 eV vs vacuum level.[16] Based on the onset reduction potentials of the polymers obtained from the cyclic voltammograms (Figure S8), the LUMO energy levels were determined (LUMO = $-(eE_{red}^{onset}$ (V vs Fc/Fc^+) + 4.8 eV)). In this way, we obtained LUMO energy levels of −3.84 eV for PNDIS-HD and 10PDI and −3.89 eV for 30PDI and 50PDI (Chart 1). The very similar LUMO energy levels of these polymers is to be expected from the similar electron-accepting strengths of the NDI and PDI moieties. Oxidation wave was not observed up to 2 V (vs SCE) in CV experiments on the acceptor polymers. Therefore, the HOMO energy levels were estimated in two ways: (i) by subtracting the E_g^{opt} from the above CV-determined LUMO energy levels and (ii) considering that the HOMO energy level of −5.95 eV was experimentally observed for NDI-biselenophene copolymer,[14a] the real HOMO energy levels of each acceptor polymer (PNDIS-HD, 10PDI, 30PDI, 50PDI) should thus be lower-lying than −5.95 eV, since selenophene is a weaker electron-donating moiety than biselenophene. We consider the HOMO energy levels (−5.95 eV) from the latter estimate to be more reliable than those from using E_g^{opt}. The HOMO/LUMO energy levels of PBDTTT-CT were also measured by using the onset oxidation/reduction potentials of CV scans, giving −5.25/−3.19 eV. These HOMO/LUMO energy levels of PBDTTT-CT provide sufficient energy offsets

DOI: 10.1021/ja513260w
J. Am. Chem. Soc. 2015, 137, 4424–4434

(>0.3 eV) with each of the acceptor polymers (PNDIS-HD, 10PDI, 30PDI, 50PDI) for efficient electron transfer[17] and hole transfer[18] essential for photovoltaic devices.

Crystallinity of Neat Polymer Films. We used wide-angle XRD analysis of thermally annealed (175 °C, 10 min) drop-casted films on glass substrates to characterize the molecular packing structure and bulk crystallinity of the new n-type copolymers (10PDI, 30PDI, and 50PDI), the reference acceptor polymer (PNDIS-HD), and the donor polymer (PBDTTT-CT) as neat films. Such solution cast films have randomly oriented crystallites which facilitate analysis and interpretation of the XRD patterns shown in Figures 2a and S9.

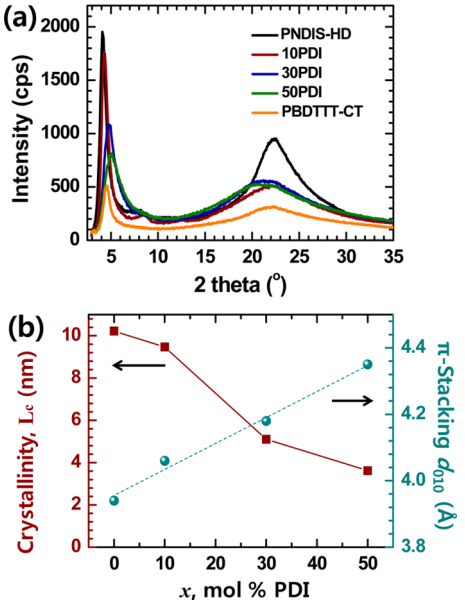

Figure 2. (a) XRD patterns of solution-casted neat films of PNDIS-HD, *x*PDIs, and PBDTTT-CT on glass substrates annealed at 175 °C for 10 min. (b) Dependence of the mean crystalline domain size (L_c) and π-stacking distance on random copolymer composition.

XRD patterns of the reference PNDIS-HD showed an intense lamellar (100) peak at $2\theta = 4.1°$ and a $\pi-\pi$ stacking (010) peak at $2\theta = 22.54°$, giving a lamellar packing distance of 21.53 Å and a $\pi-\pi$ stacking distance of 3.94 Å. The mean size of crystalline domains (L_c) was also calculated from the Scherrer equation[19] by using the full-width-at-half-maximum (fwhm) value of the lamellar (100) peak. The PNDIS-HD film has a large L_c of 10.22 nm, implying a highly crystalline film. A similar XRD analysis of the *x*PDI copolymers shows that the molecular packing and crystallinity of drop cast neat films of 10PDI, 30PDI, and 50PDI are significantly different from those of the reference PNDIS-HD. The lamellar (100) peaks of *x*PDIs are found with 2θ of 4.26°, 4.76°, and 5.08° and *d*-spacings of 20.72 Å, 18.54 Å, and 17.37 Å in 10PDI, 30PDI, and 50PDI films, respectively (Figure 2a). This represents a large progressive decrease of the lamellar *d*-spacing with increasing amount of the PDI moiety in the chain. In contrast, the $\pi-\pi$ stacking distance is increased linearly from 3.94 Å in PNDIS-HD to 4.06, 4.18, and 4.35 Å in 10PDI, 30PDI, and 50PDI films, respectively (Figure 2b). The observed progressive decrease of lamellar packing distance with increasing amount of PDI moiety results from the shorter ethylhexyl side chains on the PDI moieties and is in good agreement with similar observations when side chains of different sizes are randomly mixed in other conjugated polymer backbones.[3d,20] The progressive increase of the $\pi-\pi$ stacking distance with increasing amount of PDI moiety incorporated into the copolymer chain can be understood as a consequence of lattice distortion and decrease in polymer backbone planarity as PDI replaces some NDI units.[3d] The average crystalline domain size L_c decreased slightly from 10.22 nm in the reference PNDIS-HD to 9.47 nm in 10PDI and much more dramatically to 5.11 and 3.62 nm in 30PDI and 50PDI, respectively (Figure 2b). We conclude that random copolymerization has enabled the tuning of the bulk crystallinity of NDI/PDI-based n-type semiconducting polymers.

Table 2. XRD Data and the Mean Crystalline Domain Size (L_c) of Thermally Annealed Neat Polymers

sample	(100) (°)	d_{100} (Å)	(010) (°)	d_{010} (Å)	L_c (nm)
PBDTTT-CT	4.50	19.61	22.42	3.96	9.15
PNDIS-HD	4.10	21.53	22.54	3.94	10.22
10PDI	4.26	20.72	21.88	4.06	9.47
30PDI	4.76	18.54	21.24	4.18	5.11
50PDI	5.08	17.37	20.38	4.35	3.62

XRD patterns of the donor polymer PBDTTT-CT film showed a lamellar (100) peak at $2\theta = 4.50°$ and a $\pi-\pi$ stacking (010) peak at $2\theta = 22.42°$ with corresponding *d*-spacings of 19.61 and 3.96 Å, respectively (Figure 2a). These results are in good agreement with the previously reported XRD patterns for this polymer.[13,21] The average crystalline domain size L_c of PBDTTT-CT was found to be 9.15 nm, which is comparable with those of PNDIS-HD and 10PDI but is much larger compared to the new random copolymers 30PDI and 50PDI.

We also performed XRD analysis of the film-aged (25 °C, 96 h) electron-accepting polymer (PNDIS-HD, *x*PDIs) films to understand how film-forming conditions affect the bulk crystallinity and molecular packing. The XRD patterns are shown in Figure S10, and the data are summarized in Table S2.The lamellar (100) peaks of PNDIS-HD and *x*PDIs were found with 2θ of 4.48°, 4.88°, 5.89°, and 6.02° and *d*-spacing of 19.70, 18.09, 14.99, and 14.66 Å in PNDIS-HD, 10PDI, 30PDI, and 50PDI films, respectively. The $\pi-\pi$ stacking distance in these room-temperature-aged neat films, d_{010}, was 3.82, 3.84, 3.93, and 4.00 Å in PNDIS-HD, 10PDI, 30PDI, and 50PDI films, respectively. The trend of progressive decrease of the lamellar packing distance d_{100} with increasing amount of PDI moiety is observed similar to what was seen in the thermally annealed films. Also, similar to the observed trend in the thermally annealed films, the π-stacking distance d_{010} increased with increasing amount of the PDI moiety in the copolymer. However, the d_{100} and d_{010} spacings in the room-temperature-aged films are decreased by 9−19% and 3−8%, respectively, compared to the corresponding thermally annealed films. The average crystalline domain size L_c of these room temperature-aged films decreased from 5.22 nm in PNDIS-HD and 3.42 nm in 30PDI to 1.60 nm in 50PDI (Table S2). Thus, the observed variation of bulk crystallinity with copolymer composition is maintained under the different film-forming conditions.

Field-Effect Electron Mobility. The intrinsic electron mobility of the n-type semiconducting polymers was investigated by fabricating and testing field-effect transistors with bottom-gate and top-contact geometry.[14] The electrical parameters are summarized in Table 1, and the output and transfer characteristics are presented in Figure S13. All the new

DOI: 10.1021/ja513260w
J. Am. Chem. Soc. 2015, 137, 4424−4434

polymers (10PDI, 30PDI, and 50PDI) along with the reference PNDIS-HD showed *unipolar* n-channel characteristics and no p-channel charge transport as expected from their low-lying LUMO and HOMO energy levels (Chart 1). PNDIS-HD neat films showed the highest saturation region field-effect electron mobility of 0.092 $cm^2/(V\ s)$ with a threshold voltage (V_{th}) of 10 V and on/off ratio of 10^3; this electron mobility is comparable with the previously reported values for PNDIS-HD[6] and other NDI copolymers.[14,22] The electron mobility slightly decreased to 0.055 $cm^2/(V\ s)$ in 10PDI films, whereas it decreased substantially to 7.1×10^{-3} $cm^2/(V\ s)$ and 4.0×10^{-3} $cm^2/(V\ s)$ for 30PDI and 50PDI films, respectively. The observed trend of decreasing electron mobility from the highest value in PNDIS-HD to the lowest value in 50PDI is in excellent agreement with the XRD data which showed a progressive lowering of the crystallinity and increasing of the $\pi-\pi$ stacking distance as NDI moieties are progressively substituted with PDI moieties in the reference PNDIS-HD (Figure 2b). We also note that the observed electron mobility of $4.0 \times 10^{-3} - 0.055$ $cm^2/(V\ s)$ in neat films of the NDI/PDI random copolymers is comparable to those of other acceptor polymers used in all-polymer solar cells.[3−5]

All-Polymer BHJ Solar Cells. The photovoltaic properties of all-polymer solar cells based on *x*PDI:PBDTTT-CT (1:1 w/w) and PNDIS-HD:PBDTTT-CT (1:1 w/w) blend active layers were investigated by fabricating and evaluating diodes with the inverted structure (ITO/ZnO/polymer blend/MoO_3/Ag), and they were tested under 100 mW/cm^2 AM 1.5G solar illumination in ambient air. The polymer/polymer blend active layer was prepared under optimized conditions of spin coating from a chlorobenzene solution containing 3 vol % 1,8-diiodooctane (DIO) and aging of the blend film at room-tempaerature for 96 h to facilitate slow solvent evaporation and self-organization in an argon-filled glovebox.

The current density−voltage ($J-V$) curves and the EQE spectra of the devices are given in Figure 3a,b, respectively. The photovoltaic parameters, including the short-circuit current density (J_{sc}), the open-circuit voltage (V_{oc}), fill factor (FF), and PCE, are summarized in Table 3.

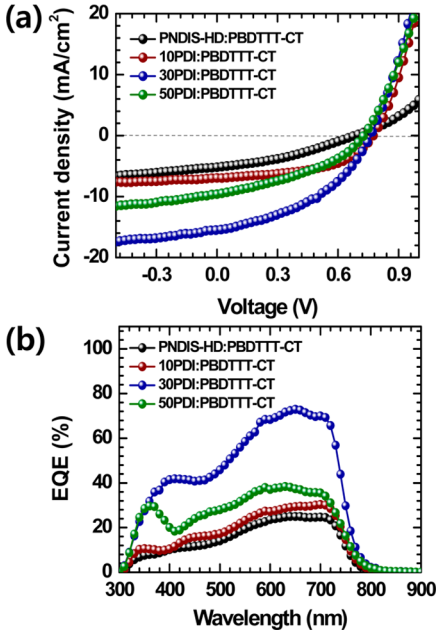

Figure 3. Current density−voltage ($J-V$) curves (a) and EQE spectra (b) of PNDIS-HD:PBDTTT-CT (1:1 w/w) and *x*PDI:PBDTTT-CT (1:1w/w) blend solar cells with film-aged (25 °C, 96 h) active layer.

The reference PNDIS-HD:PBDTTT-CT solar cells gave a maximum PCE of 1.23% with J_{sc} of 5.39 mA/cm^2, V_{oc} of 0.69, and FF of 0.35. This poor photovoltaic performance of the PNDIS-HD/PBDTTT-CT blend system means that it is incompatible. The incompatibility of this reference polymer/polymer BHJ active layer is not obvious in light of the following facts. The HOMO/LUMO energy level offsets between PNDIS-HD acceptor and PBDTTT-CT donor (Chart 1) are excellent for enabling efficient electron/hole transfer processes and charge separation.[17,18] PNDIS-HD is known to have a relatively high electron mobility (Table 1) and prior reports have showed that its blends with other donor polymers (e.g., PSEHTT) can create high efficiency all-polymer photovoltaic devices (PCE = 3−5%).[6] By virtue of its broad optical absorption in the 500−800 nm region and small optical bandgap (E_g^{opt} = 1.55 eV), the PBDTTT-CT donor has previously been used to produce high performance (PCE > 7%) polymer/[70]PCBM devices.[13] We conclude that incompatibility of PNDIS-HD/PBDTTT-CT blend system implies that these factors are not sufficient to *a priori* predict compatibility of a polymer/polymer blend pair for BHJ solar cells.

Compared to the reference PNDIS-HD:PBDTTT-CT blend system, all the new *x*PDI acceptors (10PDI, 30PDI, 50PDI), respectively, paired with the same PBDTTT-CT donor gave rise to enhanced photovoltaic performance of the BHJ devices. In the case of 10PDI:PBDTTT-CT blends, the performance of the BHJ solar cells (PCE = 2.8%, J_{sc} = 6.94 mA/cm^2, V_{oc} = 0.78 V, and FF = 0.51) is significantly improved even though the change from PNDIS-HD to 10PDI is relatively minor. A dramatic enhancement in photovoltaic performance is observed in 30PDI:PBDTTT-CT blend solar cells with V_{oc} of 0.77 V, FF of 0.43, J_{sc} of 15.55 mA/cm^2, and thus a high PCE of 5.10%. This observed efficiency in 30PDI blends represents a 4.15-fold enhancement of PCE compared to the reference PNDIS-HD blend devices. It is also to be noted that the observed photocurrent in 30PDI:PBDTTT-CT devices is comparable to those seen in the best fullerene-based $PC_{71}BM$:PBDTTT-CT solar cells[13] (15.5−17.5 mA/cm^2). Although the performance of 50PDI:PBDTTT-CT BHJ solar cells (PCE = 2.66%, J_{sc} = 9.68 mA/cm^2, V_{oc} = 0.73 V, and FF = 0.38) is still significantly higher compared to the reference PNDIS-HD devices, however, it is clear that further increase in the amount of PDI moieties in the NDI/PDI copolymers results in decrease in performance relative to the 30PDI acceptor. The dependence of the PCE on the NDI/PDI copolymer composition is shown in Figure 4, revealing that the 30 mol % PDI is the optimum.

The EQE spectra of the best *x*PDI:PBDTTT-CT and PNDIS-HD:PBDTTT-CT blend devices are shown in Figure 3b. The photoresponse of each of the blend photodiodes starts at 800 nm, which corresponds to the onset absorption of the donor polymer, and covers the entire visible region down to the UV at ~300 nm. The EQE spectra peak at about 600−700 nm, where both the p-type and n-type polymers strongly absorb. The observed EQE spectra indicate that the n-type polymer in each blend contributes to light harvesting and photocurrent generation. In the case of the 30PDI:PBDTTT-CT blend devices, the EQE peaks at 73%. We note that the photocurrent density calculated from the EQE spectra (Figure 3b) are in

DOI: 10.1021/ja513260w
J. Am. Chem. Soc. 2015, 137, 4424−4434

Table 3. Photovoltaic Properties of PNDIS-HD:PBDTTT-CT and *x*PDI:PBDTTT-CT Blend Solar Cells

blend[a]	J_{sc} (mA/cm^2)	V_{oc} (V)	FF	PCE$_{max}$ (%)	R_S (Ω cm^2)	R_{SH} (Ω cm^2)
PNDIS-HD: PBDTTT-CT	5.39 (5.19 ± 0.20)	0.69 (0.66 ± 0.02)	0.35 (0.35 ± 0.002)	1.23 (1.19 ± 0.05)	85.0	290.7
10PDI: PBDTTT-CT	6.94 (6.55 ± 0.33)	0.78 (0.77 ± 0.01)	0.51 (0.51 ± 0.005)	2.80 (2.56 ± 0.16)	19.7	616.1
30PDI: PBDTTT-CT	15.55 (15.26 ± 0.38)	0.77 (0.76 ± 0.005)	0.43 (0.42 ± 0.01)	5.10 (4.90 ± 0.17)	14.0	219.2
50PDI: PBDTTT-CT	9.68 (9.44 ± 0.25)	0.73 (0.73 ± 0.003)	0.38 (0.38 ± 0.003)	2.66 (2.58 ± 0.09)	21.9	199.2
PNDIS-HD: PBDTTT-CT[b]	4.16 (4.13 ± 0.03)	0.81 (0.80 ± 0.01)	0.40 (0.39 ± 0.01)	1.36 (1.31 ± 0.05)	18.2	211.5
30PDI: PBDTTT-CT[b]	18.55 (18.22 ± 0.28)	0.79 (0.78 ± 0.002)	0.45 (0.43 ± 0.01)	6.29 (6.17 ± 0.10)	11.3	160.6

[a]The photovoltaic properties were averaged over 10 devices. [b]ZnO layer modified by a spin-coated polyethylenimine (PEI) interfacial layer.

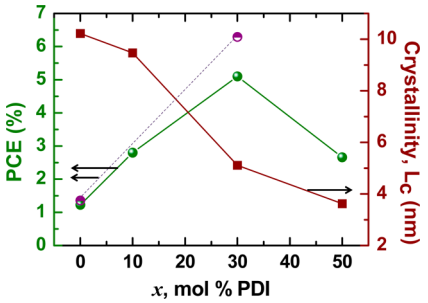

Figure 4. Dependence of PCE and the mean crystalline domain size (L_c) on random copolymer composition. Half-filled purple circles are the PCE of the devices with PEI interfacial layer modified ZnO layer.

good agreement with the J_{sc} values measured directly from the $J-V$ curves in Figure 3a.

The 30PDI:PBDTTT-CT blend and the reference PNDIS-HD:PBDTTT-CT blend devices were further optimized by using a polyethylenimine (PEI) surface modifier on the top of the zinc oxide (ZnO) layer which is known to lower the cathode work-function and thus can provide better electron injection and collection.[23] The $J-V$ curve and EQE spectrum of the 30PDI:PBDTTT-CT blend devices are shown in Figure 5, and a summary of the photovoltaic parameters is given in Table 3. A large increase in short-circuit current density (18.55 mA/cm^2) is observed with V_{oc} of 0.79 V and FF of 0.45, leading to a PCE of 6.29%. The EQE spectrum of the 30PDI:PBDTTT-CT photodiode (Figure 5b) has a maximum of 91% at 650 nm. The calculated J_{sc} from the EQE spectrum is 17.47 mA/cm^2, which is in good agreement (5.8% mismatch) with that from the $J-V$ measurement (18.55 mA/cm^2). The best performance of the reference PNDIS-HD:PBDTTT-CT blend devices with PEI-modified ZnO layer (PCE = 1.36%, J_{sc} = 4.16 mA/cm^2, V_{oc} = 0.82 V, and FF = 0.40) is only slightly improved relative to devices without the PEI interlayer. Thus, the photovoltaic efficiency of the 30PDI blend devices is 4.6-fold enhanced compared to the reference PNDIS-HD blend cells. We note that the photocurrent (18.55 mA/cm^2), PCE (6.29%), and EQE (91%) seen in the present 30PDI:PBDTTT-CT BHJ solar cells are the best observed to date in all-polymer solar cells.[3−6] Furthermore, the short-circuit current density (J_{sc} = 18.55 mA/cm^2) and EQE (91%) are also the highest measured for the donor polymer PBDTTT-CT, including PC$_{71}$BM:PBDTTT-CT devices.[13]

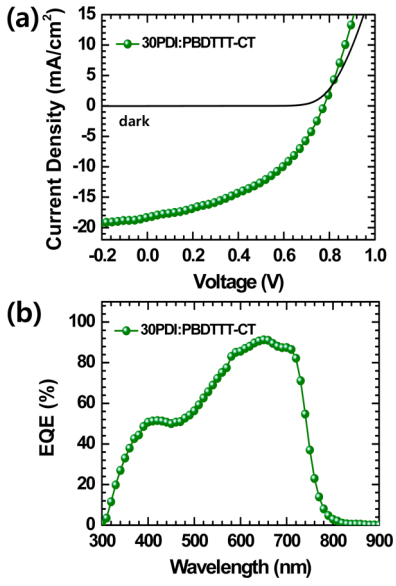

Figure 5. Current density−voltage ($J-V$) curve (a) and EQE spectrum (b) of 30PDI:PBDTTT-CT (1:1 w/w) blend solar cells with film-aged (25 °C, 96 h) active layer and a PEI interfacial layer modified ZnO layer.

The observed high PCE (6.29%) of the 30PDI:PBDTTT-CT BHJ solar cells implies that this polymer/polymer blend system is definitely compatible, whereas the reference PNDIS-HD:PBDTTT-CT blend is not. Given the far inferior photovoltaic properties of the 10PDI:PBDTTT-CT and 50PDI:PBDTTT-CT blends, compared to the 30PDI blends, we conclude that they are also incompatible like the reference PNDIS-HD blends. The dependence of the crystallinity (i.e., average crystalline domain size L_c) on copolymer composition shown in Figure 4b suggests that there is an *optimum bulk crystallinity* of the acceptor polymer (L_c = 5.11 nm for 30PDI) that facilitates its compatibility in blends with a given donor polymer (PBDTTT-CT). The fact that the crystallinity in 50PDI (L_c = 3.62 nm), which pairs with PBDTTT-CT to produce incompatible blends, is much smaller than in 30PDI, which partners with the same donor polymer to produce compatible blends, highlights our use of random copolymerization as a facile means to discover the optimum bulk crystallinity of the acceptor polymer essential to compatibility. Although these results demonstrate that bulk crystallinity of the acceptor polymer paired with a given donor polymer (PBDTTT-CT) is a critical factor that dictates compatibility and photovoltaic efficiency, the detailed mechanism of how an optimal crystallinity endows blend compatibility and enhances performance of photovoltaic devices is not yet clear, and its elucidation would require much future studies on various blend pairs. Nevertheless, we believe that the optimal crystallinity exerts its influence through the bulk morphology and bulk charge transport of the polymer/polymer blend systems as will be further discussed in subsequent sections.

Finally, we compare the observed best photovoltaic properties of 30PDI:PBDTTT-CT blends (PCE = 6.29%, J_{sc} = 18.55 mA/cm^2, V_{oc} = 0.79 V, and FF = 0.45) with those reported for

DOI: 10.1021/ja513260w
J. Am. Chem. Soc. 2015, 137, 4424−4434

the best $PC_{71}BM$:PBDTTT-CT blends.[13] As already pointed out above, the measured short-circuit current density in the present all-polymer photodiodes is significantly higher than the maximum J_{sc} (15.5−17.7 mA/cm^2) observed in $PC_{71}BM$:PBDTTT-CT,[13] while the V_{oc} is also slightly higher. However, much higher power conversion efficiencies (6.91−7.59%) and FFs (58.7−59.5%) have been reported for the $PC_{71}BM$ devices.[13] The low FF (45%) is the main limitation of the efficiency of 30PDI:PBDTTT-CT BHJ solar cells. Indeed, if FFs comparable to the $PC_{71}BM$ device values (e.g., 59.5%) could be obtained in the 30PDI:PBDTTT-CT blend devices, PCEs exceeding 8% and thus comparable to the corresponding fullerene-based solar cells would be achieved. The observed much higher maximum EQE (91%) for 30PDI:PBDTTT-CT blend devices compared to 66% for $PC_{71}BM$:PBDTTT-CT[13] suggests feasibility of such high PCEs if the low FF due to recombination losses could be addressed by further device optimization, including exploration of methods of facilitating vertical phase segregation.[24]

Morphology of BHJ Solar Cells. The surface and bulk morphologies of the *x*PDI:PBDTTT-CT (1:1 w/w) blend films as well as the reference PNDIS-HD:PBDTTT-CT (1:1 w/w) blend films prepared in identical ways as for the solar cells (film aged at room temperature for 96 h in an argon-filled glovebox) were investigated by AFM and bright-field transmission electron microscopy (BF-TEM) imaging, respectively. AFM height and phase images (1 μm × 1 μm) are shown in Figure 6. The reference PNDIS-HD:PBDTTT-CT blend films showed the largest phase-separated domains (~200 nm) with a roughness of 2.25 nm, indicating a strong tendency of the two components to phase separate into large domains. A dramatic change in the blend surface morphology is observed by increasing the amorphous PDI-selenophene component and thus decreasing the crystallinity of the acceptor polymer paired with PBDTTT-CT. First, the surface roughness decreased from 2.25 nm in PNDIS-HD blends to 1.61 and 0.62 nm in 10PDI and 30PDI blends, respectively. Second, the phase-separated domain sizes observed in *x*PDI:PBDTTT-CT blends decreased significanlty compared to the PNDIS-HD:PBDTTT-CT blends. Although crystallinity (L_c = 9.47 nm) of 10PDI is only slightly lower than that of PNDIS-HD (L_c = 10.22 nm), the observed phase-separated domain sizes (~100 nm) in the 10PDI:PBDTTT-CT blend morphology is decreased by half, indicating that small differences in the crystallinity of the component polymers can have a large impact on the surface morphology of the blends. In the case of 30PDI:PBDTTT-CT blends, a uniform phase-separated morphology with domains of about 20 nm in size was observed, and domain size was estimated from 200 × 200 nm^2 phase images (Figure S11). However, a clear phase-separated microstructure with distinct domains was not observed in the 50PDI:PBDTTT-CT blends; a surface roughness of 0.33 nm was determined from the AFM height image of this blend. The phase-separated microstructure with ~20 nm distinct domain sizes observed in the surface morphology of 30PDI:PBDTTT-CT blends (Figures 6c,g and S11) is consistent with the observed high-performance photovoltaic devices and our above earlier conclusion that this blend system is compatible. We note that based on the previously discussed photovoltaic properties, we concluded that the 50PDI:PBDTTT-CT blend system is incompatible; the AFM images of the surface morphology of this blend do not reveal a phase-separated microstructure with distinct domains, implying that its incompatibility may originate elsewhere. Overall, these results of AFM imaging demonstrate that the surface morphology of polymer/polymer blend solar cells is controlled by the crystallinity of the components, which in turn is controlled by the NDI/PDI random copolymer composition.

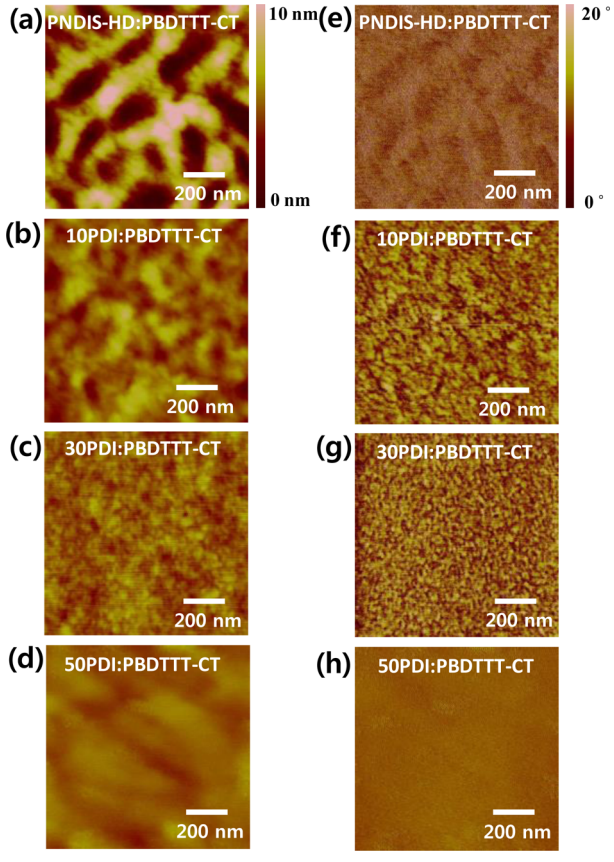

Figure 6. AFM height (a−d) and phase (e−h) images (1 μm × 1 μm) of PNDIS-HD:PBDTTT-CT (1:1 w/w) and *x*PDI:PBDTTT-CT (1:1 w/w) blend solar cells.

The BF-TEM images of the bulk morphologies of similarly prepared polymer/polymer blends are shown in Figures 7 and S12. The overall trend of phase-separated domains in the blends decreasing in size progressively from PNDIS-HD to 50PDI blends is seen in the BF-TEM results similar to the trend seen in the AFM images. In the PNDIS-HD:PBDTTT-CT blend film, isolated domains with sizes of about 200 nm are observed (Figure 7a). Such isolated domains could act as a charge trap, impede charge transport, and act as recombination centers and thus may explain the incompatibility and the poor photovoltaic properties of PNDIS-HD:PBDTTT-CT blends. In general, the *x*PDI:PBDTTT-CT blends showed much smaller and better interconnected phases compared to the PNDIS-HD blends. The 10PDI blend has significantly decreased phase-separated domain sizes (~100 nm), while the 30PDI blend has phases separated on the scale of 20 nm. In the 50PDI:PBDTTT-CT blends, however, a clear contrast between two phases is not observed (Figure 7d). The observed well interconnected nanoscale domain in the bulk morphology of 30PDI:PBDTTT-CT blend as seen in the BF-TEM image (Figure 7c) is consistent with compatibility of this blend system and its excellent photovoltaic properties. From these results, we conclude that the bulk morphology of polymer/polymer blend solar cells can be controlled by tuning the crystallinity of one of the polymer components.

DOI: 10.1021/ja513260w
J. Am. Chem. Soc. 2015, 137, 4424−4434

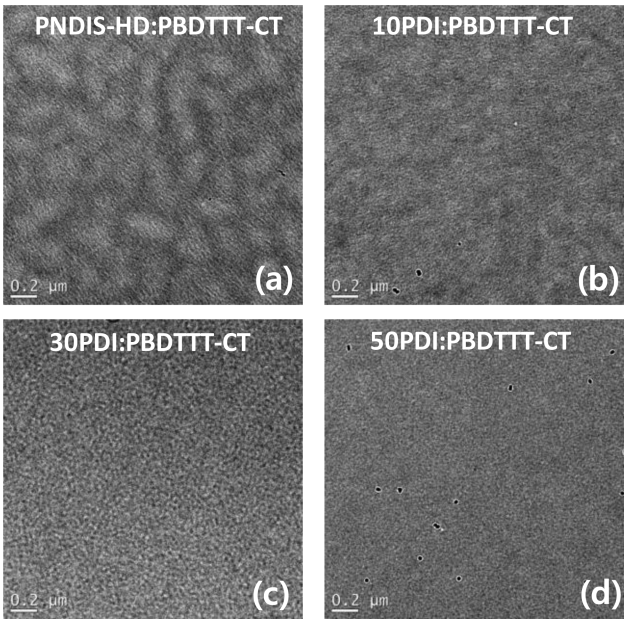

Figure 7. BF-TEM images of PNDIS-HD:PBDTTT-CT (1:1 w/w) and *x*PDI:PBDTTT-CT (1:1 w/w) blend films.

Bulk Charge Transport in BHJ Blend Films. We investigated the bulk charge carrier mobilities in the polymer/polymer blend films, which were prepared similarly to the photovoltaic devices, by using SCLC measurement. The electron mobility was measured in an ITO/ZnO/active layer/LiF/Al device structure, and the hole mobility was measured in an ITO/PEDOT:PSS/active layer/Au device structure. The current–voltage curves and SCLC fittings of the data are shown in Figure 8 and the bulk carrier mobilities are summarized in Tables S3 and S4.

The observed bulk hole and electron mobilities in the polymer/polymer blends (Tables S3 and S4) were found to vary substantially with crystallinity of the acceptor polymer component and thus with the copolymer composition. The reference PNDIS-HD:PBDTTT-CT blend systems have low bulk hole and electron mobilities of 7.5×10^{-4} and 7.2×10^{-5} $cm^2/(V\ s)$, respectively, and this result can be understood from the observed blend morphology in which large phase-separated isolated domains are not interconnected. These low and unbalanced bulk charge carrier mobilities (μ_h/μ_e = 2.6) of PNDIS-HD:PBDTTT-CT blends can explain the poor performance of the solar cells.

Compared to the reference PNDIS-HD blends, the *x*PDI:PBDTTT-CT blends showed significantly enhanced bulk charge carrier mobilities. The hole mobility of *x*PDI/PBDTTT-CT blends varied from 6.0×10^{-4} $cm^2/(V\ s)$ in 50PDI to 1.7×10^{-3} $cm^2/(V\ s)$ in 10PDI and to 2.6×10^{-3} $cm^2/(V\ s)$ in 30PDI. The hole mobility in 30PDI blends is enhanced by a factor of 3.3 compared to the hole mobility in the reference PNDIS-HD blends. Clearly, the bulk morphology in 30PDI:PBDTTT-CT is more favorable to hole transport in this blend than in either PNDIS-HD or 10PDI or 50PDI blends even though the donor polymer is identical in all the blends. The bulk electron mobility varied from 1.8×10^{-4} $cm^2/(V\ s)$ in 50PDI blends to 8.5×10^{-4} $cm^2/(V\ s)$ in 10PDI blends and to 1.0×10^{-3} $cm^2/(V\ s)$ in 30PDI blends. It is to be noted that electron mobility in 30PDI blends has increased by a factor of 13.8 compared to the electron mobility in the reference

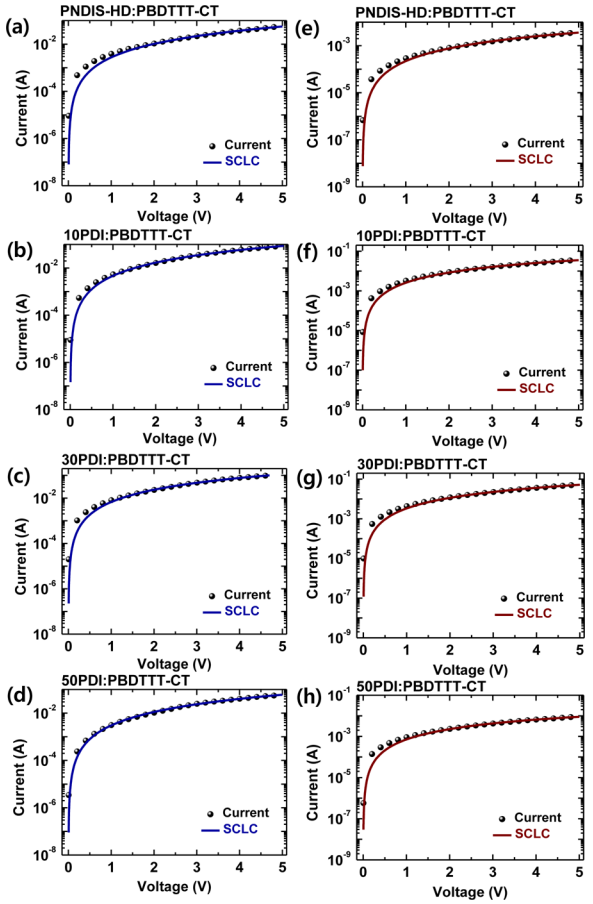

Figure 8. Current–voltage curves and SCLC fittings of PNDIS-HD:PBDTTT-CT and *x*PDI:PBDTTT-CT blend films. Hole-only SCLC devices (a–d): ITO/PEDOT:PSS/blend/Au and electron-only SCLC devices (e–h): ITO/ZnO/blend/LiF/Al.

PNDIS-HD blends. We point out that both electron and hole mobilities are highest and the carrier asymmetry (μ_h/μ_e = 2.6) lowest in the 30PDI:PBDTTT-CT blends, which are highly beneficial to high photocurrent and conversion efficiency in the BHJ solar cells. These results can be understood in terms of the previously discussed bulk morphology as imaged by BF-TEM (Figure 7), which revealed a phase-separated, interconnected microstructure with small (~20 nm) domains in 30PDI:PBDTTT-CT blends.

It is very instructive that the trends observed in the field-effect electron mobility of neat films (Table 1) of the acceptor polymers (PNDIS-HD, 10PDI, 30PDI, and 50PDI), in which μ_e decreased monotonically from PNDIS-HD to 50PDI, are not observed in the bulk electron transport in the blends. This means that the electron mobility of neat films *per se* could not be a useful guide in selecting components that would form compatible blends in all-polymer solar cells. However, the present results demonstrate that the bulk crystallinity, quantified here in terms of L_c, could be used as an important criterion in selecting compatible donor/acceptor pairs in polymer/polymer blend solar cells.

■ CONCLUSIONS

Our study has investigated the problem of how to control the crystallinity of the acceptor polymer component of polymer/polymer blend solar cells and its impact on blend compatibility, blend morphology, and performance of all-polymer solar cells.

DOI: 10.1021/ja513260w
J. Am. Chem. Soc. 2015, 137, 4424–4434

We have found that the crystallinity (e.g., L_c) of new n-type semiconducting NDI/PDI-selenophene random copolymers xPDI (x = 10, 30, 50 mol % PDI), synthesized by Stille copolymerization, varies with the copolymer composition, which thus provides a synthetic means of controlling the crystallinity of a polymer component of BHJ solar cells. Blends of the reference crystalline (L_c = 10.22 nm) acceptor polymer PNDIS-HD with crystalline (L_c = 9.47 nm) donor polymer PBDTTT-CT were found to be incompatible with poor photovoltaic properties (PCE = 1.4%). However, similar blends of the new NDI/PDI copolymer (30PDI) acceptor with optimal crystallinity (L_c = 5.11 nm) and the same PBDTTT-CT were found to be compatible with substantially enhanced photovoltaic properties (PCE = 6.3%, J_{sc} = 18.6 mA/cm^2, and EQE = 91%), which are the highest to date for all-polymer solar cells. Indeed, the observed J_{sc} and EQE in 30PDI:PBDTTT-CT blend solar cells are higher than reported values for $PC_{71}BM$:PBDTTT-CT devices.

AFM and BF-TEM imaging of the surface and bulk morphologies of the various polymer/polymer blends found that the blend microstructure varied substantially with the crystallinity of the acceptor polymer component. Both surface and bulk morphologies of the reference PNDIS-HD:PBDTTT-CT blends revealed a phase-separated microstructure with large (~200 nm) isolated domains, whereas the 30PDI:PBDTTT-CT blends have a phase-separated microstructure with small (~20 nm) interconnected domains. The bulk hole (μ_h) and electron (μ_e) mobilities and carrier asymmetry (μ_h/μ_e) in the polymer/polymer blends varied dramatically with crystallinity of the acceptor polymer component, reaching their optimal values at the optimum crystallinity found in 30PDI. The results of this study demonstrate that the bulk crystallinity of a polymer component in polymer/polymer blend solar cells is a critical factor that determines blend compatibility, blend morphology, and photovoltaic properties; furthermore, this crystallinity can be controlled by molecular design. The bulk crystallinity quantified here in terms of the average crystalline domain size L_c is a material property that can be used as an important criterion for selecting donor/acceptor pairs in polymer/polymer blend solar cells.

EXPERIMENTAL SECTION

Materials. 4,9-Dibromo-2,7-bis(2-hexyldecyl)benzo[*lmn*][3,8]-phenanthroline-1,3,6,8-tetraone (NDI) and 2,5-bis(trimethylstannyl)-selenophene were synthesized according to the known literature procedures.[6] *N*,*N*′-bis(2-ethylhexyl)-1,7-dibromo-3,4,9,10-perylene diimide (PDI) was purchased from Sunatech Inc., and the donor polymer PBDTTT-CT (M_n > 20 kDa, M_w/M_n ~ 3) was purchased from Solarmer Energy, Inc., and both were used as received. The ZnO precursor solution was prepared by dissolving 1 g of zinc acetate dihydrate (99.999% trace metals basis, Aldrich) in 10 mL of 2-methoxyethanol (99.8%, anhydrous, Aldrich) with 0.28 g of ethanolamine (≥99.5%, Aldrich) as a surfactant and stirring overnight under ambient conditions.

Poly{([*N*,*N*′-bis(2-hexyldecyl)-naphthalene-1,4,5,8-bis-(dicarboximide)-2,6-diyl]-*alt*-5,5′-selenophene)-*ran*-([N,N′-bis(2-ethylhexyl)-1,7-dibromo-3,4,9,10-perylene diimide]-*alt*-5,5′-selenophene))} (10PDI, 30PDI, and 50PDI). In the case of 10PDI, NDI (250 mg, 0.286 mmol), PDI (22.42 mg, 0.0318 mmol), and 2,5-bis(trimethylstannyl)selenophene (145.12 mg, 0.318 mmol) with $Pd_2(dba)_3$ (5.82 mg, 2 mol %) and P(o-tolyl)$_3$ (7.74 mg, 8 mol %) were added into a 100 mL three-neck round-bottom flask. The flask equipped with a condenser was then degassed and filled with argon three times. Afterward, 12.6 mL of chlorobenzene was added and degassed one time. The highly concentrated reaction mixture (34 mg/mL) was refluxed under magnetic bar stirring for 72 h under argon and cooled down to room temperature. The polymerization mixture was poured into 200 mL methanol and 5 mL hydrochloric acid solution and stirred overnight. The polymer precipitated out as a solid and was filtered using a filter paper. The polymer was purified by Soxhlet extraction with methanol, acetone, and hexane, sequentially. 10PDI (260 mg; yield = 98%), GPC: M_w = 57.2 kDa, M_n = 44.0 kDa, M_w/M_n = 1.3; TGA: T_d = 400 °C.

30PDI: NDI (250 mg, 0.286 mmol), PDI (94.83 mg, 0.123 mmol), and 2,5-bis(trimethylstannyl)selenophene (186.8 mg, 0.409 mmol) with $Pd_2(dba)_3$ (7.5 mg, 2 mol %) and P(*o*-tolyl)$_3$ (9.96 mg, 8 mol %) in 16 mL of chlorobenzene. 30PDI (329 mg; yield =97.6%), GPC: M_w = 52.5 kDa, M_n = 37.5 kDa, M_w/M_n = 1.4; TGA: T_d = 420 °C.

50PDI: NDI (169.5 mg, 0.194 mmol), PDI (150 mg, 0.194 mmol), and 2,5-bis(trimethylstannyl)selenophene (177.2 mg, 0.388 mmol) with $Pd_2(dba)_3$ (7.1 mg, 2 mol %) and P(*o*-tolyl)$_3$ (9.45 mg, 8 mol %) in 15 mL of chlorobenzene. 50PDI (305 mg; yield =98.4%), GPC: M_w = 32.1 kDa, M_n = 22.9 kDa, M_w/M_n = 1.4; TGA: T_d = 415 °C.

Characterization. The structure and physical properties of the new polymers were investigated by ^{1}H NMR, GPC analysis and TGA. ^{1}H NMR spectra at 300 MHz were recorded on a Bruker-AF300 spectrometer to verify the molecular structure, and the molecular weight was measured using a Waters 1515 GPC with a refractive index detector against polystyrene standards in *o*-dichlorobenzene at 130 °C. TGA thermograms of the polymers were acquired on a TA Instruments Q50 TGA at a heating rate of 20 °C per minute under nitrogen gas flow.

Electrochemical properties of the polymers were investigated by CV. CV experiments were done on an EG&G Princeton Applied Research potentiostat/galvanostat (model 273A) in an electrolyte solution of 0.1 M tetrabutylammonium hexafluorophosphate (Bu_4NPF_6) in acetonitrile at a scan rate of 40 m/(V s). Platinum wires were used as counter and working electrodes, and Ag/Ag$^+$ (Ag in 0.1 M $AgNO_3$ solution, Bioanalytical System, Inc.) was used as a reference electrode. Ferrocene/ferrocenium was used as an internal standard, and the reference potential was converted to the saturated calomel electrode (SCE) scale. Each sample for CV was prepared by dip-coating the copolymer solutions in chloroform onto Pt wires.

Optical absorption spectra of the polymers were measured on a PerkinElmer model Lambda 900 UV−vis/near-IR spectrophotometer. Solution- and solid-state absorption spectra were obtained from dilute (10^{-6} M) polymer solutions in chloroform and as thin films on glass substrates, respectively. Thin films (95−110 nm) were spin coated from 20 mg/mL solutions in chlorobenzene.

XRD patterns were obtained from Bruker F8 power XRD with a Cu Kα radiation as the X-ray source, and the solid samples were prepared by drop-casting of highly concentrated polymer solutions (30 mg/mL) in chloroform onto glass substrates and followed by annealing on a hot plate at 175 °C for 10 min or film-aging in an argon filled glovebox at room temperature for 96 h. The mean size of the crystalline domains (L_c) of the polymers was calculated from the lamellar peaks using the Scherrer equation, $L_c = K\lambda/\beta \cos\theta$, where K is shape factor (0.9), λ is X-ray wavelength (1.54 Å), and β is the fwhm in radian. The peak center and the fwhm were obtained by fitting the lamellar peak using Gaussian function in Origin software.

AFM and TEM Imaging. AFM characterization of surface morphology was done on the active layers of the actual BHJ solar cells by using a Veeco Dimension 3100 scanning probe microscope (SPM) system. BF-TEM images were measured on an FEI Tecnai G2 F20 TEM at 200 kV accelerating voltage and acquired with a CCD camera and recorded with Gatan Digital Micrograph software with proper exposure time (0.1 s). The TEM images were slightly defocused to enhance the phase contrast. The sample films were spin-casted on top of ITO/PEDOT:PSS substrates and peeled off by putting the samples in water. A peeled-off film was deposited on a TEM grid (Electron Microscopy Sciences, Inc.) and dried overnight in a vacuum oven.

Fabrication and Characterization of Field-Effect Transistors. A heavily n-doped silicon substrate with a 200 nm thermally grown silicon oxide layer acted as a gate electrode and insulating layer,

DOI: 10.1021/ja513260w
J. Am. Chem. Soc. 2015, 137, 4424−4434

respectively (C_i = 17 nF/cm^2). The substrate was cleaned by ultrasonication in acetone and isopropyl alcohol for 30 min each and dried under a flow of nitrogen gas. The substrate was further cleaned using ozone-plasma for 5 min. A dilute chloroform solution (0.1 M) of octyltrichlorosilane (OTS8) was spin-coated onto the silicon dioxide layer at 3000 rpm in air for 10 s. The substrates were then annealed for 10 min at 100 °C, washed with toluene, then annealed for 10 min at 150 °C. The polymer semiconductors were spin coated onto the OTS8 treated substrate from a solution in chloroform (8 mg/mL) at 2000 rpm for 60 s in an argon-filled glovebox. The films were annealed at 175 °C for 10 min, and then source/drain electrodes were deposited via thermal evaporation of silver (100 nm) that defined a channel width (W) of 1000 μm and length (L) of 100 μm. Current−voltage characteristics of the completed transistors were measured under nitrogen atmosphere using a Signatone probe station and a semiconductor parameter analyzer. The saturation region field-effect mobility (μ) and threshold voltage (V_{th}) were calculated from plots of $I_{ds}^{1/2}$ vs V_{gs} in a forward scan with V_{ds} at 80 V by using the saturation-region transistor equation: $I_{ds}= (\mu WC_i)(V_{gs} - V_{th})^2/(2L)$.

Fabrication and Characterization of All-Polymer Solar Cells. ITO glass substrates were cleaned sequentially in ultrasonic baths with acetone and isopropyl alcohol for 20 min, dried using nitrogen gas, and stored in a vacuum oven. The ITO glass substrate was O_2 plasma treated for 90 s right before coating the ZnO layer. The ZnO precursor solution was spin-coated onto the ITO glass at 5000 rpm for 40 s, annealed at 250 °C on a hot plate in air for 1 h to make 20−30 nm thick ZnO layer, and the glass/ITO/ZnO substrate was transferred into an argon-filled glovebox. A 1.0 vol % ethanolamine or 0.05 wt % PEI in 2-methoxyethanol solution was spin-coated onto the ZnO layer and dried at 110 °C on a hot plate for 10 min right before use. Each active layer (PNDIS-HD:PBDTTT-CT or xPDI:PBDTTT-CT blend (1:1 w/w) solution (25 mg/mL) in chlorobenzene with 3 vol % DIO solvent additive was spin-coated at 1000 rpm for 20 s. After spin-coating, the wet film was film-aged inside the glovebox at room temperature for 96 h (4 days) followed by thermal vacuum deposition of MoO_3 (7.5 nm) and Ag anode (100 nm). All the active layers have thicknesses of 90 ± 10 nm. Five pixels, each with an active area of 4 mm^2, were fabricated per ITO substrate. The photovoltaic cells were tested under AM 1.5G solar illumination at 100 mW/cm^2 in ambient condition using a Solar Simulator (model 16S, Solar Light Co., Philadelphia, PA) with a 200 W xenon lamp power supply (Model XPS 200, Solar Light Co., Philadelphia, PA) calibrated by NREL certified Si photodiode (Model 1787−04, Hamamatsu Photonics K.K., Japan) and a HP4155A semiconductor parameter analyzer (Yokogawa Hewlett-Packard, Japan). After the J−V measurement, the EQE was measured by using a solar cell quantum efficiency measurement system (Model QEX10, PV Measurements, Inc., Boulder, CO) with a 2 mm^2 (2 × 1 mm) size masked incident light source and TF Mini Super measurement apparatus for multiple devices in a single substrate. The EQE system was calibrated with a Si photodiode before each measurement.

SCLC Measurement. Current−voltage (J−V) characteristics of the SCLC devices were measured by using a HP4155A semiconductor parameter analyzer (Yokogawa Hewlett-Packard, Tokyo). The carrier mobility was extracted by fitting the J−V curves in the near quadratic region according to the modified Mott−Gurney equation:[25]

$$J = \frac{9}{8}\varepsilon\varepsilon_0\mu\frac{V^2}{L^3}\exp\left(0.89\beta\frac{\sqrt{V}}{\sqrt{L}}\right)$$

where J is the current density, ε_0 is the permittivity of free space, ε is the relative permittivity, μ is the zero-field mobility, V is the applied voltage, L is the thickness of active layer, and β is the field-activation factor. The SCLC device structures for electron-only and hole-only measurements were ITO/ZnO/active-layer/LiF/Al and ITO/PEDOT:PSS/active-layer/Au, respectively. Each active layer (PNDIS-HD:PBDTTT-CT or xPDI:PBDTTT-CT blend (1:1 w/w)) solution (25 mg/mL) in chlorobenzene with 3 vol % DIO solvent additive was spin-coated at 1000 rpm for 20 s. After spin-coating, the wet film was film-aged inside the glovebox at room temperature for 96 h (4 days) followed by thermal vacuum deposition of LiF (1 nm)/Al (100 nm) or Au (40 nm).

■ ASSOCIATED CONTENT

Supporting Information

Synthesis of monomers and polymers, NMR spectra, AFM images of surface morphology, output and transfer curves for field-effect transistors, and SCLC device characteristics. This material is available free of charge via the Internet at http://pubs.acs.org.

■ AUTHOR INFORMATION

Corresponding Author

*jenekhe@u.washington.edu

Notes

The authors declare no competing financial interest.

■ ACKNOWLEDGMENTS

This work was supported by the NSF (DMR-1409687) and in part by the Office of Naval Research (ONR) (N00014−11−1−0317).

■ REFERENCES

(1) (a) Halls, J. J. M.; Walsh, C. A.; Greenham, N. C.; Marseglia, E. A.; Friend, R. H.; Moratti, S. C.; Holmes, A. B. *Nature* **1995**, *376*, 498. (b) Jenekhe, S. A.; Yi, S. J. *Appl. Phys. Lett.* **2000**, *77*, 2635. (c) Alam, M. M.; Jenekhe, S. A. *Chem. Mater.* **2004**, *16*, 4647. (d) McNeill, C. R. *Energy Environ. Sci.* **2012**, *5*, 5653.

(2) (a) Ahmed, E.; Ren, G.; Kim, F. S.; Hollenbeck, E. C.; Jenekhe, S. A. *Chem. Mater.* **2011**, *23*, 4563. (b) Li, H.; Earmme, T.; Ren, G.; Saeki, A.; Yoshikawa, S.; Murari, N. M.; Subramaniyan, S.; Crane, M. J.; Seki, S.; Jenekhe, S. A. *J. Am. Chem. Soc.* **2014**, *136*, 14589. (c) Guo, X.; Facchetti, A.; Marks, T. J. *Chem. Rev.* **2014**, *114*, 8943.

(3) (a) Schubert, M.; Dolfen, D.; Frisch, J.; Roland, S.; Steyrleuthner, R.; Stiller, B.; Chen, Z.; Scherf, U.; Koch, N.; Facchetti, A.; Neher, D. *Adv. Energy Mater.* **2012**, *2*, 369. (b) Zhou, E.; Cong, J.; Hashimoto, K.; Tajima, K. *Adv. Mater.* **2013**, *25*, 6991. (c) Mori, D.; Benten, H.; Okada, I.; Ohkita, H.; Ito, S. *Energy Environ. Sci.* **2014**, *7*, 2939. (d) Hwang, Y. J.; Earmme, T.; Subramaniyan, S.; Jenekhe, S. A. *Chem. Commun.* **2014**, *50*, 10801. (e) Mori, D.; Benten, H.; Okada, I.; Ohkita, H.; Ito, S. *Adv. Energy Mater.* **2014**, *4*, 1301006. (f) Kang, H.; Kim, K. H.; Choi, J.; Lee, C.; Kim, B. J. *ACS Macro Lett.* **2014**, *3*, 1009. (g) Zhou, N.; Lin, H.; Lou, S. J.; Yu, X.; Guo, P.; Manley, E. F.; Loser, S.; Hartnett, P.; Huang, H.; Wasielewski, M. R.; Chen, L. X.; Chang, R. P. H.; Facchetti, A.; Marks, T. J. *Adv. Energy Mater.* **2014**, *4*, 1300785. (h) Mu, C.; Liu, P.; Ma, W.; Jiang, K.; Zhao, J.; Zhang, K.; Chen, Z.; Wei, Z.; Yi, Y.; Wang, J.; Yang, S.; Huang, F.; Facchetti, A.; Ade, H.; Yan, H. *Adv. Mater.* **2014**, *26*, 7224.

(4) (a) Zhan, X.; Tan, Z.; Domercq, B.; An, Z.; Zhang, X.; Barlow, S.; Li, Y.; Zhu, D.; Kippelen, B.; Marder, S. R. *J. Am. Chem. Soc.* **2007**, *129*, 7246. (b) Zhou, E.; Cong, J.; Wei, Q.; Tajima, K.; Yang, C.; Hashimoto, K. *Angew. Chem., Int. Ed.* **2011**, *50*, 2799. (c) Zhou, Y.; Yan, Q.; Zheng, Y. Q.; Wang, J. Y.; Zhao, D.; Pei, J. *J. Mater. Chem. A* **2013**, *1*, 6609. (d) Zhou, Y.; Kurosawa, T.; Ma, W.; Guo, Y.; Fang, L.; Vandewal, K.; Diao, Y.; Wang, C.; Yan, Q.; Reinspach, J.; Mei, J.; Appleton, A. L.; Koleilat, G. I.; Gao, Y.; Mannsfeld, S. C. B.; Salleo, A.; Ade, H.; Zhao, D.; Bao, Z. *Adv. Mater.* **2014**, *26*, 3767. (e) Kozycz, L. M.; Gao, D.; Tilley, A. J.; Seferos, D. S. *J. Polym. Sci., Part A: Polym. Chem.* **2014**, *52*, 3337.

(5) (a) Kietzke, T.; Horhold, H. H.; Neher, D. *Chem. Mater.* **2005**, *17*, 6532. (b) Holcombe, T. W.; Woo, C. H.; Kavulak, D. F. J.; Thompson, B. C.; Frechet, J. M. J. *J. Am. Chem. Soc.* **2009**, *131*, 14160. (c) Mori, D.; Benten, H.; Ohkita, H.; Ito, S.; Miyake, K. *ACS Appl. Mater. Interfaces* **2012**, *4*, 3325. (d) Guo, C.; Lin, Y. H.; Witman, M. D.; Smith, K. A.; Wang, C.; Hexemer, A.; Strzalka, J.; Gomez, E. D.;

DOI: 10.1021/ja513260w
J. Am. Chem. Soc. 2015, 137, 4424−4434

Verduzco, R. *Nano Lett.* **2013**, *13*, 2957. (e) Li, W.; Christian Roelofs, W. S.; Turbiez, M.; Wienk, M. M.; Janssen, R. A. J. *Adv. Mater.* **2014**, *26*, 3304. (f) Jung, I. H.; Lo, W. Y.; Jang, J.; Chen, W.; Zhao, D.; Landry, E. S.; Lu, L.; Talapin, D. V.; Yu, L. *Chem. Mater.* **2014**, *26*, 3450.
(6) (a) Earmme, T.; Hwang, Y. J.; Murari, N. M.; Subramaniyan, S.; Jenekhe, S. A. *J. Am. Chem. Soc.* **2013**, *135*, 14960. (b) Earmme, T.; Hwang, Y. J.; Subramaniyan, S.; Jenekhe, S. A. *Adv. Mater.* **2014**, *26*, 6080.
(7) (a) Small, C. E.; Chen, S.; Subbiah, J.; Amb, C. M.; Tsang, S. W.; Lai, T. H.; Reynolds, J. R.; So, F. *Nat. Photonics* **2012**, *6*, 115. (b) He, Z.; Zhong, C.; Su, S.; Wu, H.; Cao, Y. *Nat. Photonics* **2012**, *6*, 591. (c) Liao, S. H.; Jhuo, H. J.; Cheng, Y. S.; Chen, S. A. *Adv. Mater.* **2013**, *25*, 4766. (d) Cabanetos, C.; El Labban, A.; Bartelt, J. A.; Douglas, J. D.; Mateker, W. R.; Frechet, J. M. J.; McGehee, M. D.; Beaujuge, P. M. *J. Am. Chem. Soc.* **2013**, *135*, 4656. (e) Chen, J. D.; Cui, C.; Li, Y. Q.; Zhou, L.; Ou, Q. D.; Li, C.; Li, Y.; Tang, J. X. *Adv. Mater.* **2015**, *27*, 1132. (f) Xu, T.; Yu, L. *Mater. Today* **2014**, *17*, 11.
(8) (a) Anthony, J. E.; Facchetti, A.; Heeney, M.; Marder, S. R.; Zhan, X. *Adv. Mater.* **2010**, *22*, 3876. (b) Facchetti, A. *Mater. Today* **2013**, *16*, 123.
(9) (a) Utracki, L. A. *Polymer Alloys and Blends*; Hanser Publishers: New York, 1990. (b) Alam, M. M.; Tonzola, C. J.; Jenekhe, S. A. *Macromolecules* **2003**, *36*, 6577.
(10) Zhao, G.; He, Y.; Li, Y. *Adv. Mater.* **2010**, *22*, 4355.
(11) (a) Subramaniyan, S.; Xin, H.; Kim, F. S.; Shoaee, S.; Durrant, J. R.; Jenekhe, S. A. *Adv. Energy Mater.* **2011**, *1*, 854. (b) Xin, H.; Subramaniyan, S.; Kwon, T.-W.; Shoaee, S.; Durrant, J. R.; Jenekhe, S. A. *Chem. Mater.* **2012**, *24*, 1995.
(12) (a) Shoaee, S.; Subramaniyan, S.; Xin, H.; Keiderling, C.; Tuladhar, P. S.; Jamieson, F.; Jenekhe, S. A.; Durrant, J. R. *Adv. Funct. Mater.* **2013**, *23*, 3286. (b) Jamieson, F. C.; Domingo, E. B.; McCarthy-Ward, T.; Heeney, M.; Stingelin, N.; Durrant, J. R. *Chem. Sci.* **2012**, *3*, 485.
(13) (a) Huo, L.; Zhang, S.; Guo, X.; Xu, F.; Li, Y.; Hou, J. *Angew. Chem., Int. Ed.* **2011**, *50*, 9697. (b) Fan, X.; Fang, G.; Cheng, F.; Qin, P.; Huang, H.; Li, Y. *J. Phys. D: Appl. Phys.* **2013**, *46*, 305106.
(14) (a) Hwang, Y. J.; Ren, G.; Murari, N. M.; Jenekhe, S. A. *Macromolecules* **2012**, *45*, 9056. (b) Hwang, Y. J.; Murari, N. M.; Jenekhe, S. A. *Polym. Chem.* **2013**, *4*, 3187.
(15) Kronholm, D.; Hummelen, J. C. *Mater. Matters* **2007**, *2*, 16.
(16) Pavlishchuk, V. V.; Addison, A. W. *Inorg. Chim. Acta* **2000**, *298*, 97.
(17) Heeger, A. J. *Adv. Mater.* **2014**, *26*, 10.
(18) Ren, G.; Schlenker, C. W.; Ahmed, E.; Subramaniyan, S.; Olthof, S.; Kahn, A.; Ginger, D. S.; Jenekhe, S. A. *Adv. Funct. Mater.* **2013**, *23*, 1238.
(19) Patterson, A. L. *Phys. Rev.* **1939**, *56*, 978.
(20) (a) Wu, P. T.; Ren, G.; Jenekhe, S. A. *Macromolecules* **2010**, *43*, 3306. (b) Burkhart, B.; Khlyabich, P. P.; Thompson, B. C. *ACS Macro Lett.* **2012**, *1*, 660.
(21) Yan, H.; Zhu, L.; Li, D.; Zhang, Y.; Yi, Y.; Yang, Y.; Wei, Z.; Bredas, J. L. *J. Phys. Chem. C* **2014**, *118*, 29473.
(22) Guo, X.; Kim, F. S.; Seger, M. J.; Jenekhe, S. A.; Watson, M. D. *Chem. Mater.* **2012**, *24*, 1434.
(23) Zhou, Y.; Fuentes-Hernandez, C.; Shim, J.; Meyer, J.; Giordano, A. J.; Li, H.; Winget, P.; Papadopoulos, T.; Cheun, H.; Kim, J.; Fenoll, M.; Dindar, A.; Haske, W.; Najafabadi, E.; Khan, T. M.; Sojoudi, H.; Barlow, S.; Graham, S.; Bredas, J. L.; Marder, S. R.; Kahn, A.; Kippelen, B. *Science* **2012**, *336*, 327.
(24) (a) Kim, Y.; Cook, S.; Tuladhar, S. M.; Choulis, S. A.; Nelson, J.; Durrant, J. R.; Bradley, D. D. C.; Giles, M.; McCulloch, I.; Ha, C. S.; Ree, M. *Nat. Mater.* **2006**, *5*, 197. (b) Murari, N. M.; Crane, M. J.; Earmme, T.; Hwang, Y. J.; Jenekhe, S. A. *Appl. Phys. Lett.* **2014**, *104*, 223906.
(25) Mott, N. F.; Gurney, R. W. *Electronic Processes in Ionic Crystals*; Oxford University Press: London, 1940.

DOI: 10.1021/ja513260w
J. Am. Chem. Soc. 2015, 137, 4424−4434